

---

# HandSSCA: 3D Hand Mesh Reconstruction

## with State Space Channel Attention from RGB images

---

**Zixun Jiao**

Xi'an Polytechnic University

**Xihan Wang**

Xi'an Polytechnic University

**QuanliGao\***

Xi'an Polytechnic University

### Abstract

Reconstructing a hand mesh from a single RGB image is a challenging task because hands are often occluded by objects. Most previous works attempted to introduce more additional information and adopt attention mechanisms to improve 3D reconstruction results, but it would increase computational complexity. This observation prompts us to propose a new and concise architecture while improving computational efficiency. In this work, we propose a simple and effective 3D hand mesh reconstruction network HandSSCA, which is the first to incorporate state space modeling into the field of hand pose estimation. In the network, we have designed a novel state space channel attention module that extends the effective sensory field, extracts hand features in the spatial dimension, and enhances hand regional features in the channel dimension. This design helps to reconstruct a complete and detailed hand mesh. Extensive experiments conducted on well-known datasets featuring challenging hand-object occlusions (such as FREIHAND, DEXYCB, and HO3D) demonstrate that our proposed HandSSCA achieves state-of-the-art performance while maintaining a minimal parameter count.

**Keywords:** 3D hand mesh reconstruction, hand pose estimation, hand-object occlusion, computer vision

## 1. Introduction

Reconstruction of 3D hand pose from a single RGB image has a wide range of applications in many fields, such as VR/AR, robotics, and human-computer interaction. In order to reduce the cost of use in above areas, 3D hand pose estimation based on RGB images has attracted much attention due to its low cost and computational friendliness, which provides new solutions for practical applications. Influenced by the rapid development of deep learning, many excellent works [1-7] have emerged in this field. These works focus on issues related to hand-object occlusion and the loss of local information. Despite significant advancements, most methods still struggle to reconstruct hand poses in scenarios with substantial occlusion or when there is a lack of prior knowledge.

The previous methods can be broadly categorized into two groups, one is by incorporating additional a priori knowledge. For example, Zimm et al. [8] obtained hand region features via a hand segmentation network. And Wang et al. [5] added keypoint coordinates as strong a priori information to constrain hand pose. These methods can enhance pose estimation performance, but they lack essential a priori information in practical applications. Another category is to learn the intrinsic connection between image features through deep networks, Park et al. [6] extracts the

complete hand information by distinguishing the features. jiao et al. [9] uses the Transformer architecture to obtain the global information and expects to learn the hand feature mapping from the occluded part. These methods tend to mine the association between image features, but there are still some limitations. First, the Attention mechanism leads to excessive computational complexity. Second, an overload of global information can interfere with the effective receptive field [49], as shown in Fig. 1(b).

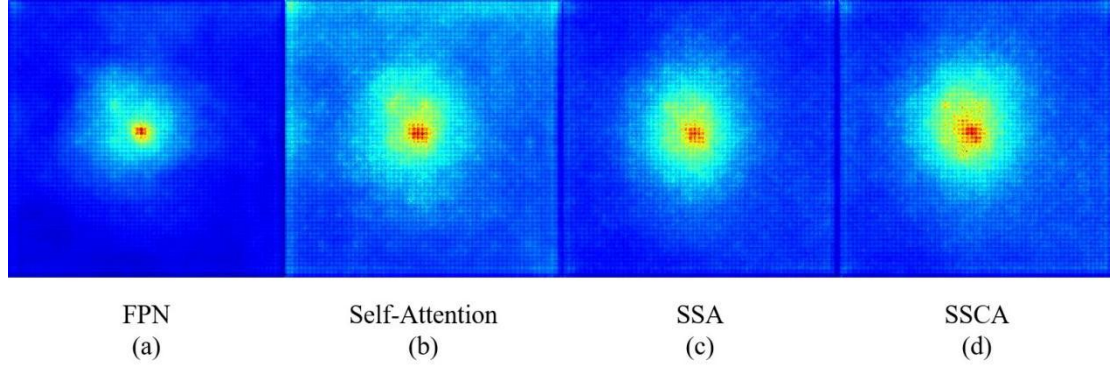


Fig. 1 Effective receptive fields (from left to right, FPN, Self-Attention, State Space Attention(SSA) and State Space Channel Attention(SSCA), respectively)

Based on the above observations, we propose a simple and effective 3D hand reconstruction network HandSSCA. This framework for the first time incorporates state space modeling [10-12] into the field of hand pose estimation. At the same time, combining the idea of spatial channel feature fusion [13], State Space Channel Attention (SSCA) was constructed, which emphasizes the contribution of channel dimension features to image features, as shown in Fig. 3. This not only increases the range of effective receptive fields in the network, but also effectively avoids the computational complexity of traditional attention square steps. Specifically, our main contributions are as follows:

(1) We propose a hand pose estimation model called HandSSCA, which introduces the concept of state space model to the field of hand pose estimation for the first time. This network can effectively improve hand reconstruction performance without the need for additional prior knowledge.

(2) We propose a spatial and channel-based parallel scanning approach to compensate for the missing channel information in planar scanning. And the state space channel attention module is constructed, which can enhance the effective receptive field range while maintaining a small number of parameters.

(3) Our method achieves state-of-the-art on three datasets, FREIHAND, DEXYCB and HO3D, with a small number of parameters.

## 2. Related work

### 2.1 State Space Model

With the proposal of attention mechanism [14], it makes more models can effectively focus on global information mapping, but its quadratic computational complexity leads to computational inefficiency in the case of long sequences. In the field of natural language processing, Albert Gu et al. [15] proposed the S4 model to optimize the state space model (SSM) by simulation in order to solve the problems of computational efficiency and long sequence dependency. However, the S4 model would process all inputs in exactly the same way, which is not in line with the practical

intuition that each sequence should receive different attention. Therefore, Albert Gu et al. [16] introduced a selection mechanism to propose the Mamba architecture (S6) to learn the parameters in the traditional state-space model, through which it is able to focus on or ignore some sequences. Compared to traditional attention computation methods, S6 enables each element in a 1-D array (e.g., a text sequence) to interact with any previously scanned samples through a compressed hidden state, effectively reducing the quadratic complexity to linear. Influenced by this idea, Yue Liu et al. [10] introduced it to vision by combining the ViT model [17] to transform images into sequences, and proposed a cross-scanning module to solve the problem of image orientation sensitivity. This approach achieves linear complexity without sacrificing the global receptive field, as shown in Fig. 1(c). In addition, some researchers [11-12] have also combined state-space modeling with traditional CNN architectures to extract multi-scale global features in U-shaped structures by state-space selection modeling, and retained the deep-level information.

## 2.2 Additional information based Methods

It is difficult to restore 3D hand gestures from RGB image features alone, and most researchers use heatmaps [2, 18-19], segmentation [8, 20], depth maps [21-23], and density maps [24-25] to incorporate additional information to help the network better learn hand features in occlusion situations. In recent years, some scholars [5, 26] combined human a priori knowledge to guide the network to focus on the target region, Wang et al. [5] proposed HandGCAT, which learns the a priori knowledge of the hand joint positions through the Knowledge-Guided Graph Convolution module, and then through the Cross-Attention Transformer to guide the network to inject joint information into the occluded region. In addition, other scholars [1, 27-30] have argued that the object pose affects the hand pose, therefore, Qi et al. [28] introduced Signed Distance Field (SDF) to reconstruct the occluded object and the hand, and this method is able to determine the grip state of the hand by estimating the object pose and then determining the hand's grasping state.

## 2.3 Attention based Methods

Attentional mechanisms have achieved great success in the field of deep learning, thanks to their ability to map long-term contextual relevance, and in the task of hand pose estimation, occluded hand features can be learned through global mapping, which in turn can effectively solve the occlusion problem [6-7, 31-33]. In establishing the global context of hand-object interaction, Pavlakos et al. [33] learn the mapping relationship between hand and occlusion from large-scale data through the ViT architecture. Cho et al. [31] obtain the features related to the region of interest from the occluded portion through cross-attention. Park et al. [6] make full use of the information of occluded region as an enhancement of image feature of the hand and refine it to get the complete hand features.

# 3. Method

## 3.1 Overview

The overall network architecture is shown in Fig. 2 and consists of Backbone, SSCA and Regressor components. Given a hand image  $I \in \mathbb{R}^{256 \times 256 \times 3}$ . First, the image information is extracted by ResNet-50 and the multi-scale features are fused layer by layer to get the feature mapping map  $F \in \mathbb{R}^{256 \times 32 \times 32}$ . Then, it is fed into the SSCA module and scanned in both spatial and channel dimensions to compute a 2D feature map and fused to obtain hand features  $H \in \mathbb{R}^{256 \times 32 \times 32}$ . Finally, the hand features  $H$  are passed to Regressor to calculate the keypoint heat

map  $HM \in \mathbb{R}^{21 \times 32 \times 32}$  to predict the keypoint coordinates and output the MANO parameters through the FC layer to obtain the final 3D hand mesh.

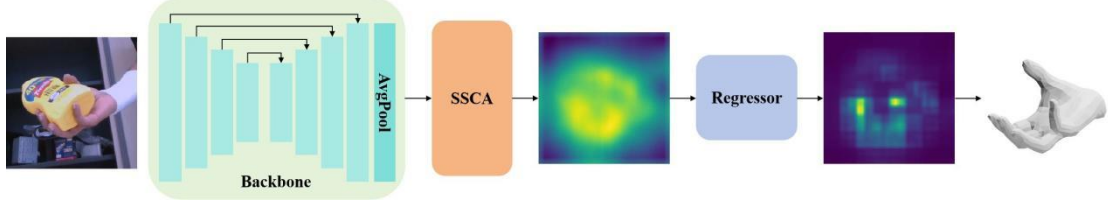


Fig. 2 Overall architecture of HandSSCA including Trunk, SSCA and Regressor. Our HandSSCA uses Resnet50 to extract image features and fuses multiscale features by upsampling layer by layer. It then uses SSCA to obtain hand region features by pairwise spatial and channel scanning. Finally, the regressor obtains keypoint information by heatmap encoding and outputs MANO parameters. The final 3D hand mesh is obtained by forwarding the MANO parameters to the MANO layer.

### 3.2 Backbone

In the feature extraction part we use ResNet-50 [34] to extract image information and fuse multi-scale features layer by layer [35]. Specifically, when the input image size is  $256 \times 256 \times 3$ , the size of the first layer of features after ResNet-50 becomes  $128 \times 128 \times 128$ . In the subsequent layers, each layer of image features  $F_i \in \frac{H_i}{2^i} \times \frac{W_i}{2^i} \times C_i$ ,  $i \in (1, 2, 3, 4)$ ,  $C_i \in (256, 512, 1024, 2048)$  is obtained by downsampling. Then, up-sampling is performed and the image features  $F_i$  are incorporated layer by layer to get the last layer of features of size  $64 \times 64 \times 256$ . Finally, the feature mapping map  $F \in \mathbb{R}^{256 \times 32 \times 32}$  is obtained by fusing the image information through average pooling.

### 3.3 State Space Channel Attention

**State Space Models.** S4ND [36] was the first study to introduce state space models into the field of vision by enabling it to receive 2D image information through a simple extension of the S4 model. The S6 module proposed by Gu et al. [16] was shown in VMamba [10] to be able to capture the global feature information of 2D image features through a selectable scanning mechanism enabling it to capture the global feature information of the 2D image features and maintain linear complexity. The state space model expects to map the input  $x(t) \in \mathbb{R}^L$  to the output  $y(t) \in \mathbb{R}^L$  through the implicit state  $h(t)$  and the parameter  $A \in \mathbb{C}^{N \times N}$ ,  $B, C \in \mathbb{C}^N$ ,  $D \in \mathbb{C}^1$  with the following equation:

$$\begin{aligned} \dot{h}(t) &= Ah(t) + Bx(t), \\ y(t) &= Ch(t) + Dx(t) \end{aligned} \quad (1)$$

In order to achieve computationally efficient operations [37], the above ordinary differential equations need to be transformed into discrete functions. Specifically, when the input size is  $X_i \in \mathbb{R}^{L \times D}$ , the discretization is performed following the following rule:

$$\begin{aligned} h_i &= \bar{A}h_{i-1} + \bar{B}x_i, \\ y_i &= \bar{C}h_i + \bar{D}x_i, \\ \bar{A} &= e^{\Delta A}, \\ \bar{B} &= (e^{\Delta A} - I)A^{-1}B, \\ \bar{C} &= C \end{aligned} \quad (2)$$

where  $B, C \in \mathbb{C}^{D \times N}$  and  $\Delta \in \mathbb{R}^D$ . In practice, we improve the  $\bar{B}$  approximation by means of a first-order Taylor series [16]:

$$\bar{B} = (e^{\Delta A} - I)A^{-1}B \approx (\Delta A)(\Delta A)^{-1}\Delta B = \Delta B \quad (3)$$

Unlike traditional spatial state models, the S6 block introduces a selective scanning mechanism, where  $B \in \mathbb{R}^{B \times L \times N}$ ,  $C \in \mathbb{R}^{B \times L \times N}$ , and  $\Delta \in \mathbb{R}^{B \times L \times D}$  can be obtained from inputs of size  $X \in \mathbb{R}^{B \times L \times D}$ . this means that S6 can sense contextual information from the inputs and update the weights.

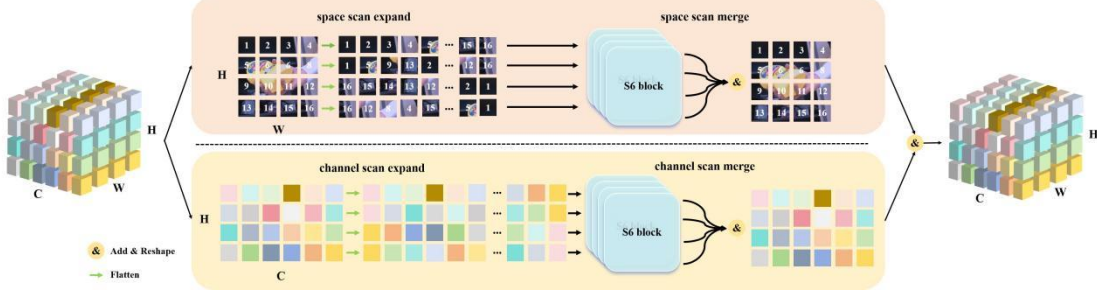


Fig. 3 SSCA module framework, we send the image features to parallel spatial and channel branches for scanning, and then process the spatial and channel resultant features and merge them through S6 block respectively, and finally sum them to get the 2D feature map.

**Space select.** Unlike textual information, image information contains 2D spatial information such as local texture and global structure, and it is difficult to obtain the contextual relationship of the local sense field of an image by scanning with a simple S6 module. The 1-D convolution is extended to 2-D convolution in S4ND [36], and this approach leads to the loss of the ability to dynamically update weights based on context. In VMamba [10], rows and columns are unfolded and scanned along in four different directions: top-left to bottom-right, bottom-right to top-left, top-right to bottom-left, and bottom-left to top-right, by means of a cross-scanning module. This allows any pixel to contain contextual information from all four directions and can enhance the size of the sensory field in the  $H \times W$  plane. Then, the sequences from each of the four directions are passed through the S6 block to compute the feature map. Finally, the four sequences are merged to obtain a new sequence of the same size as the input.

**Channel select.** Although spatial features such as local texture and global structure intrinsic to 2D image features are already available through Liu et al. However, in deep image features, channels contain richer and diverse contextual information, which is mostly ignored by these methods. Therefore, we design a spatial and channel-based parallel scanning approach to compensate for the missing channel information in planar scanning, as shown in Fig. 3. We perform scan expansion and scan fusion on the  $H \times C$  plane. First, the input features are expanded on the  $H \times C$  plane and scanned from four directions to obtain the sequence  $C_1, C_2, C_3, C_4$ . Then, they are fed into the S6 block to compute the contextual correlation in the sequence by Eq. (3), respectively. Finally, the sequences are merged and reconstructed into image feature maps of the same size.

Image features are spatially selected by activating the mapping of each pixel in the spatial plane and the four directions of up, down, left and right to obtain local texture and structure information. In channel selection, the mapping relationship between different channels can be obtained to enhance the representation of similar channels in the implicit space in order to construct a wide range of global feature mappings and to enhance the scope of the sensory field. We visualized the range of effective receptive fields for different attentions, as shown in Fig 1. As can be seen in Fig 1(d), this novel state space channel attention is able to maintain a larger and deeper receptive field range and global feature mapping capability with a reduced number of

parameters and linear complexity. This is consistent with our motivation to expect that enhancing the effective receptive field can better capture hand-object information associations from image features.

### 3.4 Regressor

In Regressor, we input the hand attention features obtained from SSMA. First, a 2D heat map of each joint  $H$  is output through a simple Conv cascade. Then, a cascade of hand attention features and 2D heatmap  $HM$  is input into four residual blocks [34]. Finally, the outputs of the residual blocks are vectorized into 2048-dimensional vectors and passed to the fully-connected layer for predicting the pose parameter  $\theta \in \mathbb{R}^{48}$  and shape parameter  $\beta \in \mathbb{R}^{10}$  of the MANO. At the same time, the joint regression matrices are multiplied by the original 3D mesh  $\bar{T}$ , and the forward kinematics are applied to obtain the final 3D hand joint coordinates  $J \in \mathbb{R}^{21 \times 3}$  and the 3D hand mesh  $V \in \mathbb{R}^{778 \times 3}$ .

To train our proposed HandSSCA hand pose estimation model, we constrain the model by calculating L2 loss on MANO parameters, 2D hand keypoints, 3D hand keypoints and vertex coordinates.

$$\text{Loss} = \alpha_\theta \|\theta^* - \theta\| + \alpha_\beta \|\beta^* - \beta\| + \alpha_{2d} \|J_{2d}^* - J_{2d}\| + \alpha_{3d} \|J_{3d}^* - J_{3d}\| + \alpha_V \|V^* - V\| \quad (4)$$

Where  $*$  denotes the true value,  $*$  denotes the predicted value, and  $\alpha_\theta = 10$ ,  $\alpha_\beta = 0.1$ ,  $\alpha_{2d} = 1e2$ ,  $\alpha_{3d} = 1e4$ ,  $\alpha_V = 1e4$ . the optimal solution is obtained by minimizing this objective function for training.

Table1 COMPARISON WITH STATE-OF-THE-ART METHODS ON FREIHAND.

Method	#Params↓	PA-MPJPE↓	PA-MPVPE↓	F@5↑	F@15↑
Hasson et al.[1]	33.5M	13.3	13.3	42.9%	90.7%
ExPose[3]	-	11.8	12.2	48.4%	91.8%
Kulon et al.[41]	519.0M	8.4	8.6	61.4%	96.6%
I2L-MeshNet[42]	136.8M	7.4	7.6	68.1%	97.3%
Pose2Mesh[43]	75.0M	7.4	7.6	68.3%	97.3%
Tang et al.[44]	156.5M	6.7	<b>6.7</b>	72.4%	98.1%
Junhyeong et al.[31]	153.0M	<b>6.5</b>	-	-	<b>98.2%</b>
HandSSCA(Ours)	<b>31.8M</b>	7.6	7.0	69.0%	<b>98.2%</b>

Table2 COMPARISON WITH STATE-OF-THE-ART METHODS ON DEXYCB.

Method	#Params↓	MPJPE↓	PA-MPJPE↓
Spurr et al.[48]	-	17.34	6.83
METRO[46]	229.5M	15.24	6.99
Liu et al.[47]	34.9M	15.28	6.58
HandOccNet[6]	39.3M	14.04	5.8
HandGCAT[5]	75.8M	13.76	5.6
HandSSCA(Ours)	<b>31.8M</b>	<b>12.81</b>	<b>5.52</b>

## 4. Experiments

### 4.1 Implementation details

All implementations were done in PyTorch. We used the Adam optimizer [50], and each model was trained by annealing every 10th time starting from an initial learning rate of 10-4 learning rate to train with a batch size of 32. Both our training and testing were performed on a server with a CPU15 vCPU AMD and an RTX A5000 (24GB). All other details will be provided

in our code.

## 4.2 Datasets and evaluation metrics

**FREIHAND.** This dataset [38] presents the first massively diverse hand dataset containing 32,560 training samples with the possibility of replacing four backgrounds. Also, there are 3960 test samples under occlusion and poor lighting.

**DEXYCB.** This dataset [40] is a large-scale dataset for object grasping and contains 582K image frames grasped on 20 YCB objects. We use the official “S0” segmentation to evaluate the right hand pose.

**HO3D.** This dataset [39] is a hand-object interaction dataset with severe occlusion and contains 66,034 training samples and 11,524 test samples. The dataset provides RGB images with MANO-based hand joints and meshes and camera parameters. The test set provides only the annotations of the RGB images and the hand bounding box, and the test results can be evaluated through an online submission system.

**Evaluation metrics.** For FreiHand, we report PA-MPJPE and PA-MPVPE in mm as well as F-scores. For HO3D we report PA-MPJPE/MPVPE, AUC and F-scores returned from the official evaluation server. For DexYCB we report MPJPE and PA-MPJPE in mm.

Table3 COMPARISON WITH STATE-OF-THE-ART METHODS ON HO3D.

Method	#Params↓	PA-M PJPE↓	PA-MPJP E AUC↑	PA-MP VPE↓	PA-MPVPE AUC↑	F@5↑	F@15↑
I2L-MeshNet[42]	136.8M	11.2	77.5%	13.9	72.2%	40.9%	93.2%
Hasson et al.[45]	<b>13.2M</b>	11.0	78.0%	11.2	77.7%	46.4%	93.9%
Hampali et al.[39]	-	10.7	78.8%	10.6	79.0%	50.6%	94.2%
METRO[46]	229.5M	10.4	79.2%	11.1	77.9%	48.4%	94.6%
Liu et al.[47]	34.9M	9.9	80.3%	9.5	81.0%	<b>52.8%</b>	<b>95.6%</b>
I2UV-HandNet[25]	-	9.9	80.4%	10.1	79.9%	50.0%	94.3%
ArtiBoost[29]	25.3M	11.4	77.3%	10.9	78.2%	48.8%	94.4%
Keypoint.[4]	56.5M	10.8	78.6%	-	-	-	-
HandSSCA(Ours)	31.8M	<b>9.5</b>	<b>80.8%</b>	<b>9.5</b>	<b>81.0%</b>	51.8%	95.5%

Table 4 ABLATION RESULTS FOR THE FREIHAND

Method	PA-MPJPE↓	PA-MPVPE↓	F@5↑	F@15↑
Baseline	8.0	7.4	66.9%	97.7%
Baseline+Self-Attention	7.7	7.0	68.8%	98.1%
Baseline+SSCA	<b>7.6</b>	<b>7.0</b>	<b>69.0%</b>	<b>98.2%</b>

Table 5 ABLATION RESULTS FOR THE DEXYCB

Method	MPJPE↓	PA-MPJPE↓
Baseline	14.07	5.78
Baseline+Self-Attention	14.40	5.81
Baseline+SSCA	<b>12.81</b>	<b>5.52</b>

## 4.3 Comparisons with the State-of-the-art Methods

We compare our proposed method with several recent state-of-the-art methods on three datasets, FreiHand, DEXYCB, and HO3D, as shown in Tables 1-3. As can be seen from Table 1, our method maintains state-of-the-art performance in the F@15 metric on a smaller number of datasets, although it is slightly worse than the other methods in the PA-MPJPE metric [31, 44]. Moreover, its number of parameters shrinks by a factor of nearly 5 compared to models with

higher accuracy [31]. On the HO3D dataset, our method reduces the number of parameters by about 40% compared to recent methods [4]. Meanwhile, when the number of parameters is similar to the method of Liu et al. [47], all other metrics are greatly improved, and only the F-score metric is slightly reduced. To verify the effectiveness of our proposed method in the case of large-scale occlusion, the metrics on the DEXYCB dataset are shown in Table 2, and all the metrics outperform the recent state-of-the-art models [5]. In conclusion, the experimental results on all three datasets show that our proposed method can still be effective in estimating hand postures when a large number of occlusions are included. Moreover, the state-of-the-art performance can be maintained while reducing the number of parameters, as shown in Fig. 4.

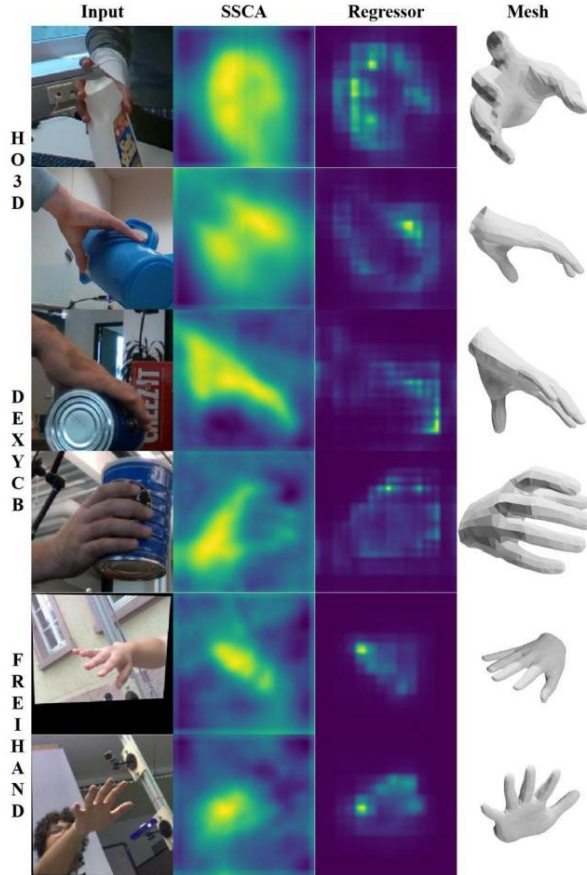


Fig. 4 Qualitative results for the three datasets. From left to right are the input image containing severe occlusions and angular distortions, the attention mapping map obtained by SSCA, the heat map of keypoints in Regressor, and the hand mesh.

Table 6 ABLATION RESULTS FOR THE HO3D

Method(#Params)	PA-MPJPE↓	PA-MPVPE↓	F@5↑	F@15↑
Baseline	9.8	9.7	51.6%	95.4%
Baseline+Self-Attention(4.6M)	10.1	10.1	50.2%	94.7%
Baseline+SSA(0.57M)	9.8	9.8	<b>52.1%</b>	95.2%
Baseline+SSCA(0.58M)	<b>9.5</b>	<b>9.5</b>	51.8%	<b>95.5%</b>

#### 4.4 Ablation Study

In order to validate the effectiveness of the HandSSCA method, we further analyzed the different attention modules. The results of the ablation experiments on different datasets are shown in Tables 4-6. On the FreiHand and DEXYCB datasets, we designed three experiments, Baseline,

Adding Self-Attention Module, and Adding SSCA Module, as a way to validate that our proposed SSCA is able to expand the effective receptive field while enhancing the hand features. On the HO3D dataset, we designed four experiments, which are Baseline, adding the self-attention module, adding the traditional state space attention module (SSA) and adding the state space channel attention module (SSCA). In this way, we demonstrate that the state space model with the addition of channel information can enhance the ability to extract hand features in the occluded state while having a wider effective receptive field.

From Tables 4 and 5, we can see that in the presence of occlusion on the hand, the global feature information obtained from the self-attention mechanism, although it can enhance the hand features to a certain extent, will introduce more noise information. In Fig. 5, we visualize the attention distribution map, and it can be clearly seen that the feature map tends to characterize the global information after adding the attention mechanism, but still does not extract the hand features well for the occluded regions and hand interaction edges. The SSA module, on the other hand, aggregates more hand information and performs better at the interaction edges, but it will characterize the occluded part as the hand, which introduces interference information to a certain extent. The SSCA module expands the range of the receptive field through the spatial plane selection mechanism, and then directionally strengthens the hand region features through the selection of the channel planes. Furthermore, by benefiting from linear directional scanning, the occluded areas are characterized using adjacent hand information, which reduces the introduction of interference through this global mapping capability.

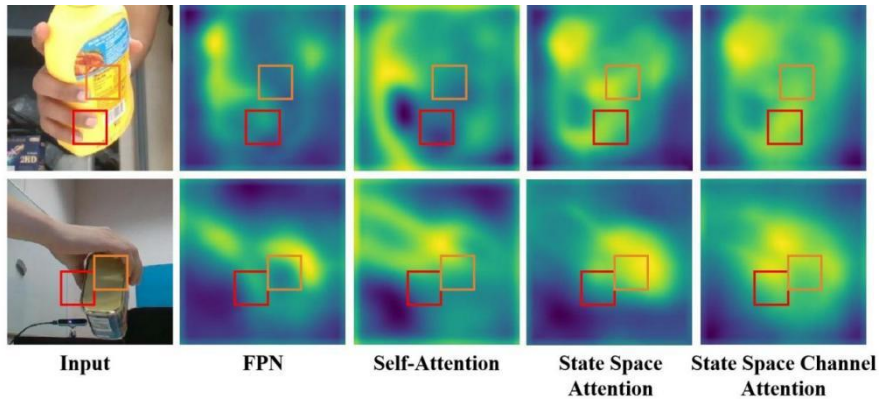


Fig. 5 Attention characterization map. It is worth noting that the SSCA module is able to obtain sufficient hand information in the hand interaction edge region and the occlusion region. And the method expands the range of the receptive field so that it can capture the global feature mapping. (Orange is the occluded region and red is the hand interaction edge region)

In Table 6, it can be found that after the introduction of the state selection of the channel plane, the number of parameters of the model is only slightly increased by 0.01M, however, a significant improvement of nearly 2% is realized in the two performance metrics of PA-MPJPE and PA-MPVPE. This is due to the fact that the state selection in the channel plane enhances the selection and fusion of image features, and is able to extract more important channel information. The current state-space model focuses more on multi-directional scanning in the spatial plane, which is the reason for the 0.3% improvement in the F@5 metrics when using SSA. Using only the spatial plane for state selection, each pixel will focus more on neighboring pixels. However, observing other metrics will show that the channel dimension in the image will then contain richer feature information, which happens to be ignored by SSA.

## 5. Conclusion

In order to effectively mitigate the challenges of the hand pose estimation task under occlusion conditions, we introduce state-space modeling into the field of hand pose estimation for the first time and propose the HandSSCA method. The method expands the effective receptive field and acquires hand features under occlusion by parallel cross-scanning in the spatial plane and the channel plane. Among them, the spatial plane is able to acquire feature associations in different directions for each pixel, and the channel plane activates the target region features through state selection. This novel attention architecture is able to acquire sufficient global information and expand the effective sensory field while keeping the number of parameters small. Extensive experimental results show that this method is able to accurately predict hand postures from heavily occluded situations. Meanwhile, we expect this spatial and channel-parallel state-selective attention architecture to make progress in different downstream tasks.

## References

- [1] Yana Hasson, Gul Varol, Dimitrios Tzionas, Igor Kalevatykh, Michael J. Black, Ivan Laptev, and Cordelia Schmid. Learning joint reconstruction of hands and manipulated objects. In ICCV, pages 11807 – 11816, 2019.
- [2] Adnane Boukhayma, Rodrigo de Bem, and Philip H.S. Torr. 3D hand shape and pose from images in the wild. In CVPR, pages 10843 – 10852, 2019.
- [3] Vasileios Choutas, Georgios Pavlakos, Timo Bolkart, Dimitrios Tzionas, and Michael J. Black. Monocular expressive body regression through body-driven attention. In ECCV, pages 20 – 40, 2020.
- [4] Shreyas Hampali, Sayan Deb Sarkar, Mahdi Rad, and Vincent Lepetit, “ Keypoint transformer: Solving joint identification in challenging hands and object interactions for accurate 3d pose estimation,” in CVPR, 2022.
- [5] Wang, Shuaibing, et al. "HandGCAT: Occlusion-Robust 3D Hand Mesh Reconstruction from Monocular Images." 2023 IEEE International Conference on Multimedia and Expo (ICME). IEEE, 2023.
- [6] JoonKyu Park, Yeonguk Oh, Gyeongsik Moon, Hongsuk Choi, and Kyoung Mu Lee, Handocnet: Occlusion-robust 3d hand mesh estimation network, in CVPR, 2022.
- [7] Li, Mengcheng et al. “ Interacting Attention Graph for Single Image Two-Hand Reconstruction.” 2022 IEEE/CVF Conference on Computer Vision and Pattern Recognition (CVPR) (2022): 2751-2760.
- [8] Zimmermann, Christiane and Thomas Brox. “Learning to Estimate 3D Hand Pose from Single RGB Images.” 2017 IEEE International Conference on Computer Vision (ICCV) (2017): 4913-4921.
- [9] Jiao Z, Wang X, Li J, et al. MTHI - former: Multilevel attention for two - handed reconstruction from RGB image[J]. Electronics Letters, 2023, 59(23): e13040.
- [10] Liu, Yue et al. “VMamba: Visual State Space Model.” ArXiv abs/2401.10166 (2024): n. pag.
- [11] Ma, Jun et al. “U-Mamba: Enhancing Long-range Dependency for Biomedical Image Segmentation.” ArXiv abs/2401.04722 (2024): n. pag.
- [12] Ruan, Jiacheng and Suncheng Xiang. “VM-UNet: Vision Mamba UNet for Medical Image Segmentation.” ArXiv abs/2402.02491 (2024): n. pag.
- [13] Hu, Jie et al. “Squeeze-and-Excitation Networks.” 2018 IEEE/CVF Conference on Computer Vision and Pattern Recognition (2017): 7132-7141.
- [14] Vaswani, Ashish et al. “Attention is All you Need.” Neural Information Processing Systems (2017).
- [15] Albert Gu, Karan Goel, and Christopher Re. Efficiently modeling long sequences with structured state spaces. In International Conference on Learning Representations, 2021.
- [16] Gu, Albert and Tri Dao. “Mamba: Linear-Time Sequence Modeling with Selective State Spaces.” ArXiv abs/2312.00752 (2023): n. pag.
- [17] Dosovitskiy, Alexey et al. “An Image is Worth 16x16 Words: Transformers for Image Recognition at Scale.” ArXiv abs/2010.11929 (2020): n. pag.
- [18] Lv, Jun et al. “HandTailor: Towards High-Precision Monocular 3D Hand Recovery.” ArXiv abs/2102.09244 (2021): n. pag.
- [19] Iqbal, Umar et al. “Hand Pose Estimation via Latent 2.5D Heatmap Regression.” European Conference on Computer Vision (2018).

- [20] Zhang, Xiong et al. "Hand Image Understanding via Deep Multi-Task Learning." 2021 IEEE/CVF International Conference on Computer Vision (ICCV) (2021): 11261-11272.
- [21] Rezaei, Mohammad et al. "TriHorn-Net: A Model for Accurate Depth-Based 3D Hand Pose Estimation." *Expert Syst. Appl.* 223 (2022): 119922.
- [22] Rezaei, Mohammad et al. "Pushing the Envelope for Depth-Based Semi-Supervised 3D Hand Pose Estimation with Consistency Training." *ArXiv abs/2303.15147* (2023): n. pag.
- [23] Wu, X., Finnegan, D., O'Neill, E., Yang, YL. (2018). HandMap: Robust Hand Pose Estimation via Intermediate Dense Guidance Map Supervision. In *ECCV 2018*. vol 11220. Springer, Cham.
- [24] Zhao, Zimeng et al. "Semi-Supervised Hand Appearance Recovery via Structure Disentanglement and Dual Adversarial Discrimination." 2023 IEEE/CVF Conference on Computer Vision and Pattern Recognition (CVPR) (2023): 12125-12136.
- [25] Chen, Ping et al. "I2UV-HandNet: Image-to-UV Prediction Network for Accurate and High-fidelity 3D Hand Mesh Modeling." 2021 IEEE/CVF International Conference on Computer Vision (ICCV) (2021): 12909-12918.
- [26] Jiang, Changlong et al. "A2J-Transformer: Anchor-to-Joint Transformer Network for 3D Interacting Hand Pose Estimation from a Single RGB Image." 2023 IEEE/CVF Conference on Computer Vision and Pattern Recognition (CVPR) (2023): 8846-8855.
- [27] Wang, Rong et al. "Interacting Hand-Object Pose Estimation via Dense Mutual Attention." 2023 IEEE/CVF Winter Conference on Applications of Computer Vision (WACV) (2022): 5724-5734.
- [28] Qi, Haozhe et al. "HOISDF: Constraining 3D Hand-Object Pose Estimation with Global Signed Distance Fields." *ArXiv abs/2402.17062* (2024): n. pag.
- [29] Li, Kailin et al. "ArtiBoost: Boosting Articulated 3D Hand-Object Pose Estimation via Online Exploration and Synthesis." 2022 IEEE/CVF Conference on Computer Vision and Pattern Recognition (CVPR) (2021): 2740-2750.
- [30] Chen, Jiayi et al. "Tracking and Reconstructing Hand Object Interactions from Point Cloud Sequences in the Wild." *AAAI Conference on Artificial Intelligence* (2022).
- [31] Cho, Junhyeong et al. "Cross-Attention of Disentangled Modalities for 3D Human Mesh Recovery with Transformers." *European Conference on Computer Vision* (2022).
- [32] Feng, Yao et al. "Collaborative Regression of Expressive Bodies using Moderation." 2021 International Conference on 3D Vision (3DV) (2021): 792-804.
- [33] Pavlakos, Georgios et al. "Reconstructing Hands in 3D with Transformers." *ArXiv abs/2312.05251* (2023): n. pag.
- [34] Kaiming He, Xiangyu Zhang, Shaoqing Ren, and Jian Sun. Deep residual learning for image recognition. In *CVPR*, 2016.
- [35] Tsung-Yi Lin, Piotr Dollár, Ross Girshick, Kaiming He, Bharath Hariharan, and Serge Belongie. Feature pyramid networks for object detection. In *CVPR*, 2017.
- [36] Nguyen, Eric et al. "S4ND: Modeling Images and Videos as Multidimensional Signals Using State Spaces." *ArXiv abs/2210.06583* (2022): n. pag.
- [37] Albert Gu, Isys Johnson, Karan Goel, Khaled Saab, Tri Dao, Atri Rudra, and Christopher Ré. Combining recurrent, convolutional, and continuous-time models with linear state space layers. *Advances in neural information processing systems*, 34:572 – 585, 2021.
- [38] Zimmermann, C., Ceylan, D., Yang, J., Russell, B.C., Argus, M., & Brox, T. (2019).

FreiHAND: A Dataset for Markerless Capture of Hand Pose and Shape From Single RGB Images. 2019 IEEE/CVF International Conference on Computer Vision (ICCV), 813-822.

[39] Shreyas Hampali, Mahdi Rad, Markus Oberweger, and Vincent Lepetit, "Honnotate: A method for 3d annotation of hand and object poses," in Proceedings of the IEEE/CVF Conference on Computer Vision and Pattern Recognition, 2020.

[40] Yu-Wei Chao, Wei Yang, Yu Xiang, Pavlo Molchanov, Ankur Handa, Jonathan Tremblay, Yashraj S. Narang, Karl Van Wyk, Umar Iqbal, Stan Birchfield, Jan Kautz, and Dieter Fox, "DexYCB: A benchmark for capturing hand grasping of objects," in Proceedings of the IEEE/CVF Conference on Computer Vision and Pattern Recognition, 2021.

[41] Dominik Kulon, Riza Alp Guler, Iasonas Kokkinos, Michael Bronstein, and Stefanos Zafeiriou. Weakly-supervised mesh convolutional hand reconstruction in the wild. In CVPR, pages 4990 – 5000, 2020.

[42] Gyeongsik Moon and Kyoung Mu Lee. I2L-MeshNet:Image-to-lixel prediction network for accurate 3D human pose and mesh estimation from a single RGB image. In ECCV, pages 752 – 768, 2020.

[43] Hongsuk Choi, Gyeongsik Moon, and Kyoung Mu Lee. Pose2Mesh: Graph convolutional network for 3D human pose and mesh recovery from a 2D human pose. In ECCV, pages 769 – 787, 2020.

[44] Xiao Tang, Tianyu Wang, and Chi-Wing Fu. Towards accurate alignment in real-time 3dD hand-mesh reconstruction. In ICCV, 2021.

[45] Yana Hasson, Bugra Tekin, Federica Bogo, Ivan Laptev, Marc Pollefeys, and Cordelia Schmid, "Leveraging photometric consistency over time for sparsely supervised hand-object reconstruction," in CVPR, 2020.

[46] Kevin Lin, Lijuan Wang, and Zicheng Liu, "End-to-end human pose and mesh reconstruction with transformers," in CVPR, 2021.

[47] Shaowei Liu, Hanwen Jiang, Jiarui Xu, Sifei Liu, and Xiaolong Wang, "Semi-supervised 3d hand-object poses estimation with interactions in time," in CVPR, 2021.

[48] Adrian Spurr, Umar Iqbal, Pavlo Molchanov, Otmar Hilliges, and Jan Kautz, Weakly supervised 3d hand pose estimation via biomechanical constraints, in Proceedings of the European Conference on Computer Vision (ECCV). Springer, 2020.

[49] Luo, Wenjie et al. "Understanding the Effective Receptive Field in Deep Convolutional Neural Networks." ArXiv abs/1701.04128 (2016): n. pag.

[50] Diederik P Kingma and Jimmy Ba. Adam: A method for stochastic optimization. In ICLR, 2015.